J Appl Electrochem (2009) 39:2007–2013
DOI 10.1007/s10800-009-9911-5

ORIGINAL PAPER

Study of electrochemical properties and the charge/discharge mechanism for $Li_4Mn_5O_{12}/MnO_2$-AC hybrid supercapacitor

Hong Yan Chu · Qiong Yu Lai · Yan Jing Hao · Yan Zhao · Xiao Yun Xu

Received: 13 December 2008 / Accepted: 14 April 2009 / Published online: 30 April 2009

Abstract Spinel $Li_4Mn_5O_{12}$ was prepared by a sol–gel method. The manganese oxide and activated carbon composite (MnO_2-AC) were prepared by a method in which $KMnO_4$ was reduced by activated carbon (AC). The products were characterized by XRD and FTIR. The hybrid supercapacitor was fabricated with $Li_4Mn_5O_{12}$ and MnO_2-AC, which were used as materials of the two electrodes. The pseudocapacitance performance of the $Li_4Mn_5O_{12}/MnO_2$-AC hybrid supercapacitor was studied in various aqueous electrolytes. Electrochemical properties of the $Li_4Mn_5O_{12}/MnO_2$-AC hybrid supercapacitor were studied by using cyclic voltammetry, electrochemical impedance measurement, and galvanostatic charge/discharge tests. The results show that the hybrid supercapacitor has electrochemical capacitance performance. The charge/discharge test showed that the specific capacitance of 51.3 F g^{-1} was obtained within potential range of 0–1.3 V at a charge/discharge current density of 100 mA g^{-1} in 1 mol L^{-1} Li_2SO_4 solution. The charge/discharge mechanism of $Li_4Mn_5O_{12}$ and MnO_2-AC was discussed.

Keywords $Li_4Mn_5O_{12}$ · MnO_2-AC · Hybrid supercapacitor · Electrochemical property · Mechanism

1 Introduction

Electrochemical capacitors (ECs), which were also called supercapacitors, are intermediate devices between conventional dielectric capacitors and batteries that deliver high power and high circle counts. Much more attention has been devoted to develop supercapacitors due to their high specific power and potential applications in many fields such as hybrid electric vehicles, power sources, portable electronic devices, and space flight technology in recent years [1]. Two basic types of supercapacitors can be realized by using different charge storage mechanisms [1, 2]: (a) electrochemical double layer capacitance (EDLC) rules show charge/discharge of the non-Faradaic electrical double layers due to charge separation on the electrode material–electrolyte interface, which employ carbon or other similar materials as blocking electrodes [3, 4]; (b) redox pseudocapacitance rules show the charge transfer of electroactive species within electrode materials through Faradaic redox reactions (e.g., RuO_2, MnO_2, CoO, NiO, V_2O_5 etc. [5–12]).

Compared with other carbon materials, activated carbon (AC) has some advantages such as accessibility, easy processability, relatively low cost, excellent stability, and so on. Considering all these characteristics mentioned, AC employed as a material for the storage of energy in supercapacitor is commendably attractive. However, AC capacitor has quite lower specific capacitance which could limit their practical application. MnO_2 is a promising supercapacitor material due to good electrochemical performance, high specific capacitance, low cost of the raw material, and environmental friendly nature. Therefore, the combination of these two may be result in both the faradaic capacitance of the metal oxide and the double layer capacitance of the carbon.

In recent years, based on lithium-ion insertion extraction, some lithium-transition oxide materials have been used in supercapacitors. A study on a new concept $LiMn_2O_4$/carbon hybrid supercapacitor using mild Li_2SO_4 aqueous electrolyte was reported [13]. The device exhibits two different

H. Y. Chu · Q. Y. Lai (✉) · Y. J. Hao · Y. Zhao · X. Y. Xu
College of Chemistry, Sichuan University, Chengdu 610064, People's Republic of China
e-mail: laiqy5@hotmail.com

charge storage mechanisms. An EDLC rules the negative-activated carbon electrode, while the lithium insertion compound electrode shows the insertion/extraction of Li-ions. Pasquier et al. [14] had reported that the asymmetric hybrid capacitors used $Li_4Ti_5O_{12}$ and poly (methyl) thiophene (PMeT) as the negative and positive electrodes, respectively, was investigated in 2 mol L^{-1} $LiBF_4$ in CH_3CN electrolyte. $LiNi_{1/3}Co_{1/3}Mn_{1/3}O_2$ and $LiCoO_2$ are also used as electrode materials for supercapacitor [15, 16].

In the present study, a hybrid supercapacitor was fabricated with a MnO_2-AC composite material and $Li_4Mn_5O_{12}$ as electrode materials in an aqueous electrolyte system. The charge/discharge mechanism of $Li_4Mn_5O_{12}$ and MnO_2-AC was discussed. The combination of $Li_4Mn_5O_{12}$ and MnO_2-AC in aqueous electrolyte shows good cycle life and the use of aqueous electrolyte can prevent the drawbacks of safety hazards from the use of highly toxic and flammable organic solvents.

2 Experimental

2.1 Synthesize of $Li_4Mn_5O_{12}$

The $Li_4Mn_5O_{12}$ particles were synthesized by a sol–gel process. Required amount of $LiOH \cdot 2H_2O$ (AR) and $Mn(CH_3COO)_2 \cdot 4H_2O$ (AR) was dissolved in distilled water with the molar ratio of Li:Mn = 4:5 and then certain amount of citric acid was added to this solution at 75 °C under water bath with constantly stirring. Aqueous ammonia was slowly added to this mixture solution until the pH value reached 6.5. The solution was then heated at 75 °C until a gel formed. The resulting gel was dried at 100 °C under vacuum to extract out excessive water and yielded a dry precursor, which was preheated at 300 °C in air for 2 h to decompose the citric acid and further calcined at 500 °C for 8 h to obtain the final product.

2.2 Preparation of MnO_2-AC composite material

In this experiment, 1.0 g of pristine AC was blended with 100 mL of 0.3 mol L^{-1} $KMnO_4$ solution in a 250 mL three-necked round-bottomed flask. The flask was placed at constant temperature oil bath. The suspension containing AC was then refluxed at 140 °C using sustained magnetic stirring. After 12 h, the mixture was filtered and washed with distilled water several times. Finally, The MnO_2 that was prepared by the redox reaction and the residual AC formed MnO_2-AC composite products.

2.3 Characterization of the samples

The $Li_4Mn_5O_{12}$ and MnO_2-AC sample were determined by X-ray diffraction (XRD). XRD data was collected on a RigakuD/MAX–rA diffractometer with Cu Kα radiation, operating at 40 kV and 100 mA. The Fourier transform infrared (FT-IR) spectrum was recorded by a Nicolet 170SX spectrometer with KBr.

2.4 Electrochemical measurements

Composite electrodes were prepared by mixing the active material $Li_4Mn_5O_{12}$ in NMP with acetylene black, and polyvinylidene fluoride (PVDF) dried powders in the following weight ratios: 70:25:5. The mixture was pressed onto stainless steel grids and then dried for 24 h at 60 °C under vacuum. MnO_2-AC composite electrode was prepared with the same procedure described above. All the work were done at room temperature.

The cyclic voltammetry test was performed by using LK2005 electrochemical workstation system in 1 mol L^{-1} Li_2SO_4, Na_2SO_4, and K_2SO_4. The $Li_4Mn_5O_{12}$ (or the MnO_2-AC composite), platinum foil, and saturated calomel electrode (SCE) were served as working electrode, counter electrode, and reference electrode, respectively. Charge/discharge performance of the hybrid capacitors was performed by using Neware battery program-control testing system in two-electrode system. Electrochemical impedance spectroscopy (EIS) was performed in a three-electrode cell setup with the $Li_4Mn_5O_{12}$ (or the MnO_2-AC composite) as the working electrode, platinum foil as counter, and SCE as the reference. It was performed by Potentiostat Galvanostat PGSTAT302 (The Netherlands) in 1 mol L^{-1} Li_2SO_4 solution.

3 Results and discussions

3.1 X-ray diffraction analysis

Figure 1 shows XRD pattern of the prepared $Li_4Mn_5O_{12}$ sample. The XRD pattern of the prepared sample is agreement with JCPDS card (no. 46-0810). The results indicate that the sample is spinel $Li_4Mn_5O_{12}$ that belongs to Fd3m space group. The $Li_4Mn_5O_{12}$ with a spinel-framework structure can be expressed as: $[Li]_{8a}[Li_{0.33}Mn_{1.67}]_{16d}[O_4]_{32e}$. Such a structure provides a three-dimensional tunnel for Li^+ insertion and extraction with minimal change in the unit-cell volume [17]. The pattern demonstrates the good crystalline structure due to the sharp diffraction peaks, which is propitious to Li-ion inserting into/expelling out.

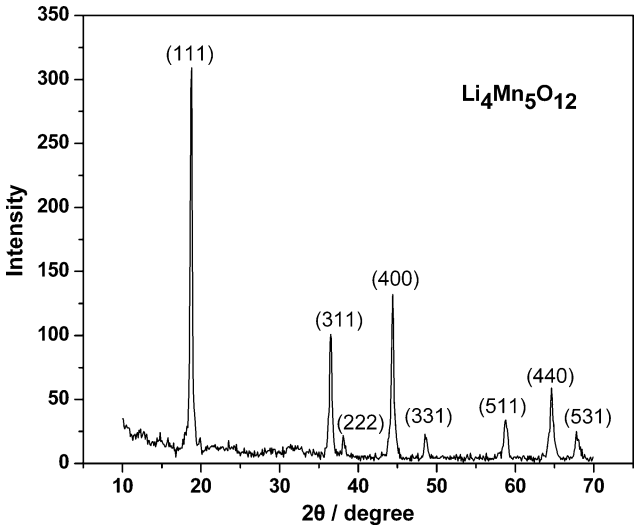

Fig. 1 XRD pattern of the prepared $Li_4Mn_5O_{12}$ sample

Structural investigation (Fig. 2) indicates that the MnO_2-AC composite sample is amorphous. A more amorphous structure has been considered to be favorable in increasing the specific capacitance of the oxide electrode for the supercapacitor [18]. The highly amorphous structure should favor the insertion/extraction of ions the oxide matrix, which can increase contact between the electrolyte and the electrode material and improve the utilization ratio of the material. Insertion/extraction of ions will result in dilation of an oxide lattice, but the lattice is difficult to change in crystalline structure, however, the amorphous structure can be rearranged when the ions are inserted. Therefore, amorphous structure is favorable in increasing the specific capacitance of the oxide electrode.

3.2 IR analysis

Figure 3 shows the Fourier transform infrared spectrum (FTIR) patterns for the MnO_2 (a) and the MnO_2-AC (b) sample. Several absorption bands in Fig. 3b can be observed at 3421, 1627, 1410, 1119, 571 and 530 cm^{-1}, respectively. The 3,421 cm^{-1} band should be attributed to the O–H stretching vibration, and the 1627, 1410 and 1119 cm^{-1} bands are normally attributed to O–H bending vibrations. The 571 and 530 cm^{-1} bands should be ascribed to the Mn–O stretching vibration [19]. All absorption bands in Fig. 3b correspond with the absorption bands in Fig. 3a. The IR result indicates that the sample is MnO_2 composite.

3.3 Electrochemical analysis

3.3.1 Effect of working voltage

Since the working voltage is one of the predominant factors influencing the energy density of the hybrid supercapacitor, the working voltage of $Li_4Mn_5O_{12}$ electrode was examined by changing the potential window of CV in 0–1.3 V, 0–1.4 V, and 0–1.5 V versus SCE at a scan rate of 5 mV s^{-1} in 1 mol L^{-1} Li_2SO_4 electrolyte as can be seen in Fig. 4. In order to ensure the electrolyte not to be decomposed during charge/discharge process in aqueous system, it is important to control a safe potential window where O_2 and H_2 evolution will not appear on the electrodes surface. In Fig. 4, the peak of O_2 evolution occurs when voltage value is over 1.3 V (vs. SCE). Therefore, the safe potential window for $Li_4Mn_5O_{12}$ material is controlled between 0 and 1.3 V in 1 mol L^{-1} Li_2SO_4.

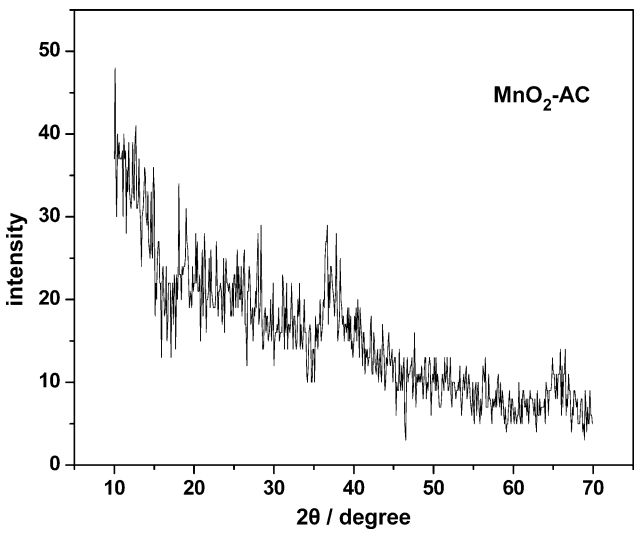

Fig. 2 XRD pattern of the prepared MnO_2-AC sample

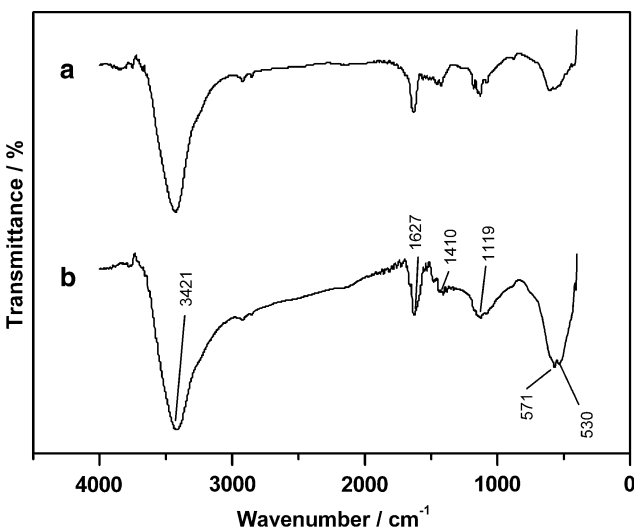

Fig. 3 FTIR spectra of **a** the MnO_2-AC sample; **b** MnO_2

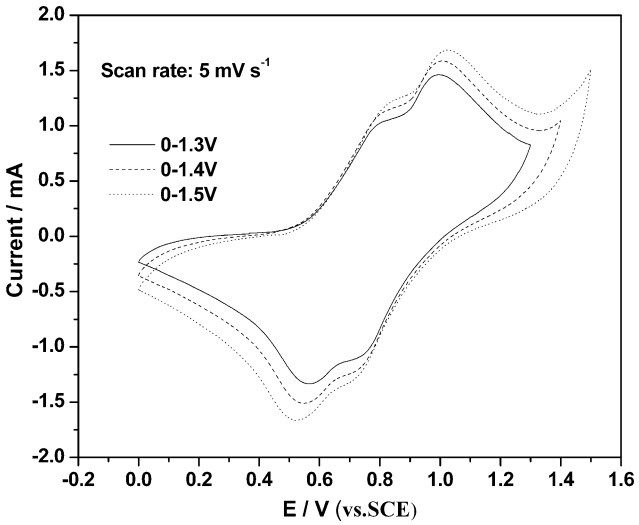

Fig. 4 CV curves of the $Li_4Mn_5O_{12}$ electrode in various potential ranges at scan rate 5 mV s^{-1} in 1 mol $L^{-1}Li_2SO_4$

3.3.2 *Effect of scan rate*

The CV curves of the $Li_4Mn_5O_{12}$ electrode at different scan rates in the potential range of 0–1.3 V (vs. SCE) in 1 mol L^{-1} Li_2SO_4 aqueous solution are recorded in Fig. 5. It exhibits obvious redox peaks below 20 mV s^{-1} scan rate, suggesting Li^+ could diffuse into the inner lattice of the material due to the small current at a low scan rate [20]. Increasing scan rate will result in a direct impact on the diffusion of Li^+ into the lattice of the $Li_4Mn_5O_{12}$ electrode material. At higher scan rates the Li-ions only approach the outer surface of the $Li_4Mn_5O_{12}$, resulting in a low utilization of active material and a smaller pseudocapacitance.

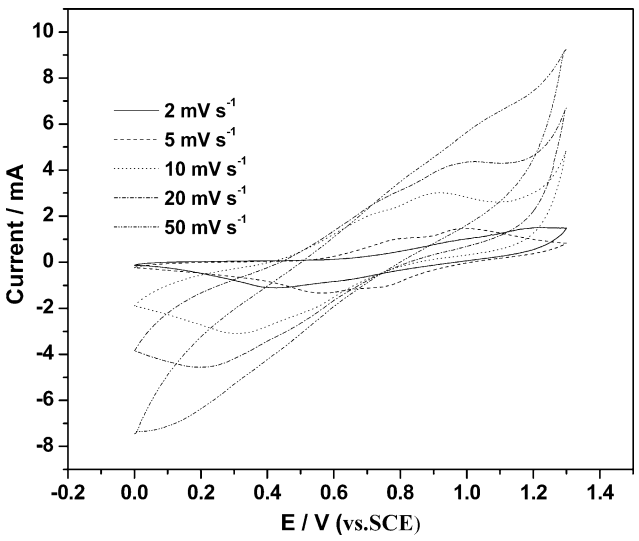

Fig. 5 CV curves of the $Li_4Mn_5O_{12}$ electrode at various scan rates in the potential range of 0–1.3 V at scan rate 5 mV s^{-1} in 1 mol L^{-1} Li_2SO_4

3.3.3 *Cyclic voltammogram analysis of MnO_2-AC electrode*

The MnO_2-AC electrode was examined at different scan rates in −0.2 to 1.0 V (vs. SCE) in 1 mol L^{-1} Li_2SO_4 that is shown in Fig. 6. On CV curves, the voltammetric responses on the positive sweep are symmetrical to those on the following negative sweep, indicating the electrochemical reversibility of the MnO_2-AC electrode is good. The CV curves are similar to rectangle in low scan rates (e.g., 5 mV s^{-1}, 10 mV s^{-1}), indicating that MnO_2-AC electrode has good pseudocapacitance performance.

3.3.4 *Effect of different electrolytes*

Figure 7 shows CV curves of the $Li_4Mn_5O_{12}$ electrode in various aqueous electrolytes at the scan rate of 100 mV s^{-1} in 0–1.3 V (vs. SCE). As can be seen in the figure, the CV curve in 1 mol L^{-1} Li_2SO_4 electrolyte has obvious redox peaks, indicating that the $Li_4Mn_5O_{12}$ electrode in 1 mol L^{-1} Li_2SO_4 electrolyte has good pseudocapacitance performance. The area encircled by CV curve in 1 mol L^{-1} Li_2SO_4 is bigger than in the other solutions, indicating that the $Li_4Mn_5O_{12}$ electrode has better capacitance performance. Therefore, in this article the most appropriate electrolyte is 1 mol L^{-1} Li_2SO_4.

The Charge/discharge curves of the hybrid supercapacitor in 1 mol L^{-1} Li_2SO_4, Na_2SO_4, and K_2SO_4 aqueous solutions at a current density of 100 mA g^{-1} are shown in Fig. 8. As can be seen in Fig. 8, the supercapacitor exhibits much better capacitive behavior in 1 mol L^{-1} Li_2SO_4 solution than that in the other solutions, indicating that the charge storage mechanism of the $Li_4Mn_5O_{12}$ electrode

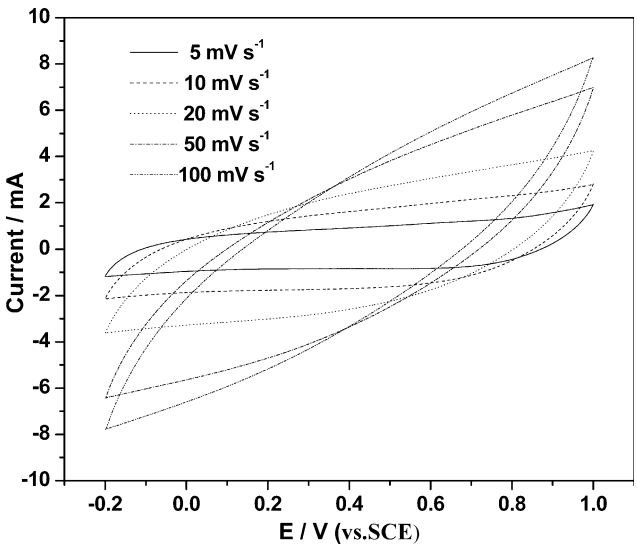

Fig. 6 CV curves of the MnO_2-AC electrode at different scan rates at −0.2–1.0 V (vs. SCE) in 1 mol L^{-1} Li_2SO_4

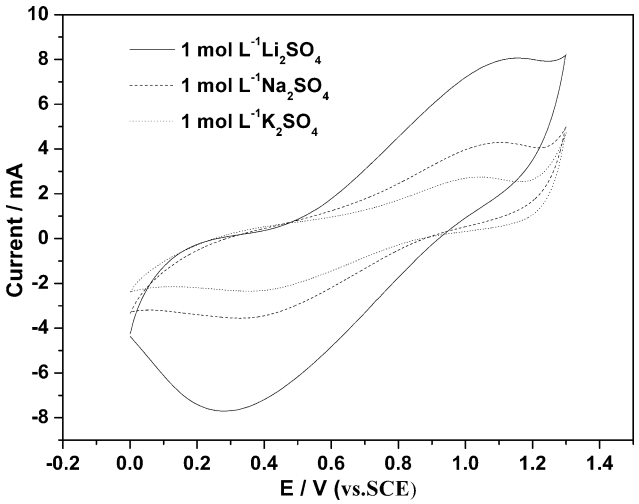

Fig. 7 CV curves of the $Li_4Mn_5O_{12}$ electrode in various aqueous electrolytes at scan rate 100 mV s^{-1}in the potential range of 0–1.3 V (vs. SCE) 1 mol L^{-1} Li_2SO_4

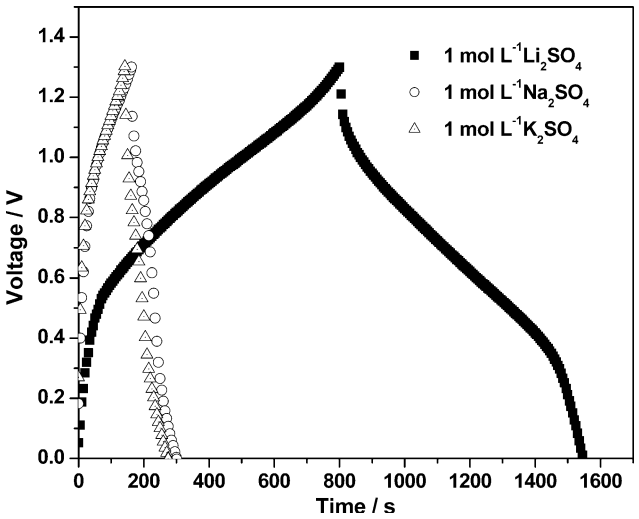

Fig. 8 Charge/discharge curves of the $Li_4Mn_5O_{12}/MnO_2$-AC hybrid supercapacitor in various aqueous electrolytes

material in aqueous electrolyte is interrelated with the insertion/extraction of Li-ions, which is about the same as the charge storage mechanism of $Li_4Mn_5O_{12}$ material in organic electrolyte. The $Li_4Mn_5O_{12}$ with a spinel framework structure can be expressed as: $[Li]_{8a}[Li_{0.33}Mn_{1.67}]_{16d}[O_4]_{32e}$. Such a structure could be favorable to the insertion/extraction of Li^+ ions. During discharge process, Li-ions first intercalate into 16d sites in $Li_4Mn_5O_{12}$ spinel structure, even intercalating into the tetrahedral 8a sites, also migrate to 16d sites. Eventually, the 16d sites are occupied by Li-ions. As demonstrated above, a charge–discharge mechanism based on the concept of Li^+ ion intercalation is proposed for the $Li_4Mn_5O_{12}$ electrode, can be proposed as follows:

$$Li_{4+x}Mn_5O_{12} \underset{discharge}{\overset{charge}{\rightleftharpoons}} Li_4Mn_5O_{12} + xLi^+ + xe \quad (1)$$

During the charge process, Li-ions in spinel $Li_{4+x}Mn_5O_{12}$ material are easily deinserted to form $Li_4Mn_5O_{12}$, leading to the appearance of many Li-ion vacant sites in the electrode material. During the discharge process, it is difficult for K^+ and Na^+ in electrolyte solution to reinsert into the vacant sites because of their larger sizes. Therefore, Li_2SO_4 solution is used for testing in this article.

The charge/discharge mechanism of MnO_2 in Li_2SO_4 aqueous solution is complicated, it can be described commonly as following reversible reactions (2) and (3) [21, 22].

$$MnO_2 + H^+ + e \underset{Discharge}{\overset{Charge}{\rightleftharpoons}} MnOOH \quad (2)$$

$$MnO_2 + Li^+ + e \underset{Discharge}{\overset{Charge}{\rightleftharpoons}} MnOOLi \quad (3)$$

3.3.5 *Calculation of the discharge specific capacitance*

The charge/discharge curves of the $Li_4Mn_5O_{12}/MnO_2$-AC hybrid supercapacitor at a constant current density of 100 mA g^{-1} in 1 mol L^{-1} Li_2SO_4 are shown in Fig. 9. As can be seen in Fig. 9, the slope of charge/discharge curves almost keeps constant, indicating $Li_4Mn_5O_{12}$ electrode has higher electrochemical reversibility and excellent capacitive characteristic.

The discharge specific capacitance (C_s) of hybrid capacitor was calculated from the below formula:

$$C_s = \frac{dQ}{mdV} = \frac{dQdt}{mdtdV} \approx \frac{I\Delta t}{m\Delta V} \quad (4)$$

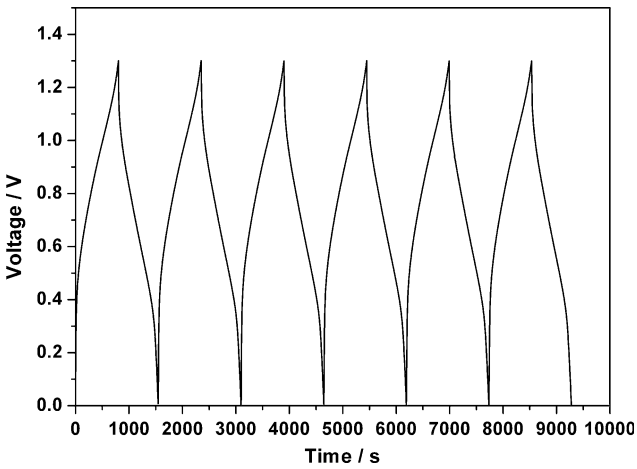

Fig. 9 Charge/discharge curve of the $Li_4Mn_5O_{12}/MnO_2$-AC hybrid supercapacitor at a constant current density of 100 mA g^{-1} in 1 mol L^{-1} Li_2SO_4

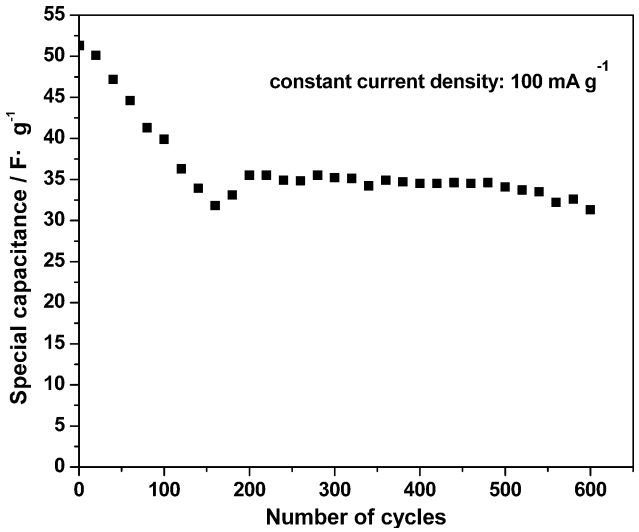

Fig. 10 Variation of discharge specific capacitance within potential range of 0–1.3 V at a charge/discharge current density of 100 mA g^{-1} in 1 mol L^{-1} Li_2SO_4 with respect to cycle number

where I (A), ΔV (V), Δt (s), and m are the discharge current, discharge potential range, discharge time consumed in the potential range, and the active mass of the two electrodes, respectively. The hybrid supercapacitor shows the specific capacitance 51.3 F g^{-1} within potential range of 0–1.3 V at a charge/discharge current density of 100 mA g^{-1} in 1 mol L^{-1} Li_2SO_4 electrolyte.

Charge/discharge studies were performed at a constant current of 100 mA g^{-1} between 0 and 1.3 V and discharge specific capacitance for 600 cycles is shown in Fig. 10. $Li_4Mn_5O_{12}$/MnO_2-AC hybrid supercapacitor delivered the initial special capacitance of 51.3 F g^{-1} at a current density of 100 mA g^{-1} in 1 mol L^{-1} Li_2SO_4 electrolyte. The discharge specific capacitance value of the hybrid supercapacitor remained 31.3 F g^{-1} after 600 cycles, exhibiting a good cycling performance and the structure stability.

3.3.6 *Electrochemical impedance analysis*

The Nyquist impedance spectra of $Li_4Mn_5O_{12}$ electrode and MnO_2-AC electrode are shown in Fig. 11a and b, respectively. The frequency responses of an electrode material can be clearly characterized by investigating the electrochemical impedance spectra (EIS). The high frequency intercept on the real axis provides the solution or electrolyte resistance (Re) and the diameter of semicircle provides the electronic resistance (Rm) of the electrode materials, which arises from diffusion of counter ions between the electrolyte and the electrode materials. The Nyquist impedance spectra in Fig. 11a consist of a high frequency semicircle and a low frequency spike. The Re is very small as can be seen from the Fig. 11a, indicating that 1 mol L^{-1} Li_2SO_4 electrolyte is appropriate for $Li_4Mn_5O_{12}$ electrode. The $Li_4Mn_5O_{12}$ electrode resistance (Rm_1) is about 41.3 ohm. For the $Li_4Mn_5O_{12}$ electrode, the low frequency spike shows an inclination at an angle $\sim$70°, indicating that the electrode in 1 mol L^{-1} Li_2SO_4 has good capacitive behavior. The Nyquist impedance spectra in Fig. 11b typically consist of a high frequency arc of a one-fourth and a low frequency spike. Re is about 1.8 ohm in Fig. 11b, while the MnO_2-AC electrode resistance (Rm_2) is about 18.1 ohm. For the MnO_2-AC electrode, the low frequency spike shows an inclination at an angle $\sim$60°, indicating that the electrode in 1 mol L^{-1} Li_2SO_4 has good capacitive behavior [23]. Moreover, the discharge specific capacitance of the $Li_4Mn_5O_{12}$ electrode and the MnO_2-AC electrode can be calculated from Eq. 5 in low frequency range, respectively [24].

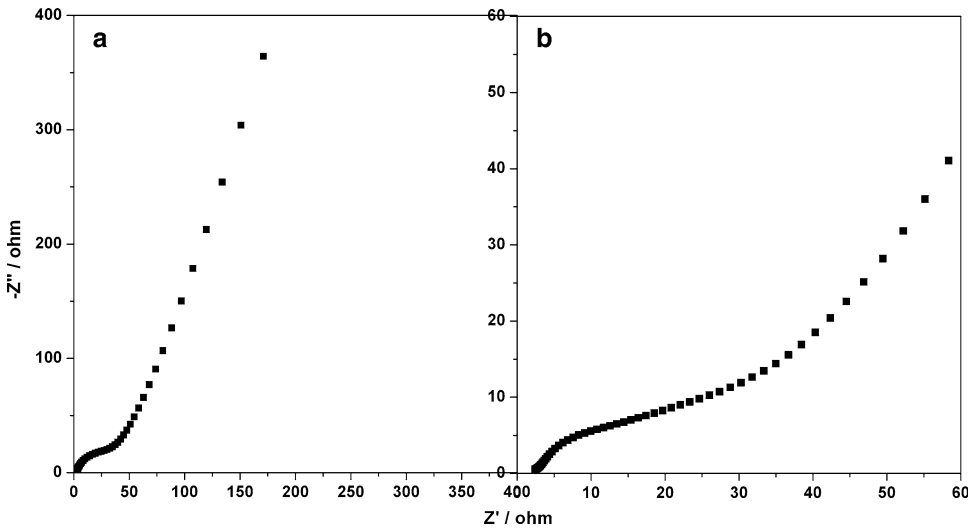

Fig. 11 The Nyquist impedance spectra of the electrodes in 1 mol L^{-1} Li_2SO_4 **a** $Li_4Mn_5O_{12}$; **b** MnO_2-AC

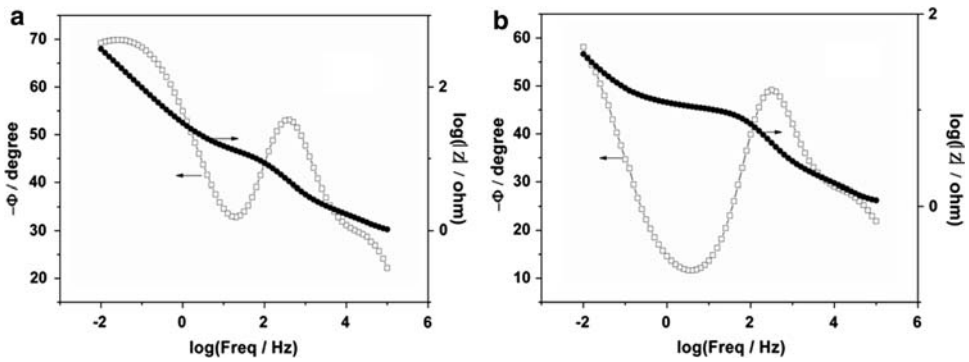

Fig. 12 The Bode plots for the electrodes in 1 mol L^{-1} Li_2SO_4 **a** $Li_4Mn_5O_{12}$; **b** MnO_2-AC

$$C_s = -\frac{1}{2\pi f m Z''} \quad (5)$$

where f, m, Z'' are the frequency of the low-frequency range (Hz), here the low frequency is 0.01 Hz, mass of the electrodes (g), and the impedance of the imaginary part (ohm), respectively. The specific capacitance of two electrodes calculated from the Z'' value at the lowest frequency (0.01 Hz) is 50.3 and 194.2 F g^{-1}, respectively.

The bode plots for the $Li_4Mn_5O_{12}$ electrode and the MnO_2-AC electrode are shown in Fig. 12a and b. As can be seen in Fig. 12a and b, the total impedance of increases with decrease in the frequency. In the lower frequency (0.01 Hz), the negative values of the phase angle reach $-60°$, $-70°$ for the $Li_4Mn_5O_{12}$ electrode and the MnO_2-AC electrode, respectively. These values of phase angle indicate that the both electrode material has good capacitive behavior [25].

4 Conclusion

In this work, a sol–gel method was used to prepare $Li_4Mn_5O_{12}$ powders, and the manganese oxide-activated carbon composite (MnO_2-AC) was prepared by a method in which $KMnO_4$ was reduced by activated carbon. A hybrid supercapacitor in which $Li_4Mn_5O_{12}$ and MnO_2-AC were used as electrode materials was fabricated. Its electrochemical properties were tested by cyclic voltammetry, charge/discharge test, and impedance spectroscopy measurement. The results showed that potential range, scan rate, and species of aqueous electrolyte had great effect on the capacitive properties of the $Li_4Mn_5O_{12}$/MnO_2-AC hybrid supercapacitor. Charge/discharge mechanisms of $Li_4Mn_5O_{12}$ and MnO_2-AC in aqueous electrolyte were discussed. In the potential range of 0–1.3 V, the hybrid supercapacitor delivered a discharge specific capacitance of 51.3 F g^{-1} within potential range of 0–1.3 V at a charge/discharge current density of 100 mA g^{-1} in 1 mol L^{-1} Li_2SO_4 electrolyte.

Acknowledgment The authors acknowledge the financial support from the National Natural Science Foundation of China (no. 20701029).

References

1. Conway BE (2005) Electrochemical supercapacitors-scientific fundamentals and technological applications (Chen A, Wu MQ, Zhang XL, Gao NW trans.). Chemistry Industry Press, Beijing
2. Sarangapani S, Tilak BV, Chen CP (1996) J Electrochem Soc 143:3791
3. Ishikawa M, Morita M, Ihara M et al (1994) J Electrochem Soc 141:1730
4. Mayer ST, Pekala RW et al (1993) J ElectrochemSoc 140:446
5. Zhang JP, Cygon PJ, Jow TR (1995) J Electochem Soc 142:2699
6. Zhang JP, Jow TR, Jia QX et al (1996) J Electochem Soc 143:1068
7. Chang K, Hu C (2004) J Electrochem Soc 151:A958
8. Lee HY, Goodenough JB (1999) J Solid State Chem 144:220
9. Brousse T, Toupin M, Dugas R et al (1999) J Electrochem Soc 153:A2171
10. Kim H, Seong T, Lim J et al (2001) J Power Sources 102:167
11. Nam K, Yoon W, Kim K (2002) Electrochim Acta 47:3201
12. Kudo T, Ikeda Y, Watanabe T et al (2002) Solid State Ion 152–153:833
13. Wang YG, Xia YY (2005) Electrochem Commun 7:1138
14. Pasquier AD, Laforgue A, Simon P (2004) J Power Sources 125:95
15. Wang YG, Lou JY, Wu W et al (2007) J Electrochem Soc 154:A228
16. Wang YG, Lou JY, Wang CX (2006) J Electrochem Soc 153:A1425
17. Wang GX, Zhong S, Bradhurst DH et al (1998) J Power Sources 74:198
18. Hu CC, Tsou TW (2003) J Power Sources 115:179
19. Yuan AB, Zhang QL (2006) Electrochem Commun 8:1173
20. Chang JK, Tsai WT (2003) J Electrochem Soc 150:A1333
21. Wu MQ, Snook GA, Chen GZ et al (2004) Electrochem Commun 6:499
22. Chen Y, Zhang ML, Shi ZH (2005) J Electrochem Soc 152:A1272
23. Subramanian V, Zhang HW, Wei BQ (2006) Electrochem Commun 8:827
24. Lufrano F, Staiti P (2004) Electrochim Acta 49:2683
25. Zhang GQ, Zhao YQ, Feng Tao et al (2006) J Power Sources 161:723